NMR Imaging of Saturation during Immiscible Displacements

The use of magnetic resonance imaging (MRI) for monitoring multiphase displacement experiments for quantitative characterization of fluid saturations is demonstrated. Displacements are conducted with one fluid phase in a porous medium being immiscibly displaced by another. Our objective is to accurately measure porosity and saturation distributions corresponding to one spatial dimension. Measures for the accuracy and resolution, with which the properties are identified, are developed.

Shanthi S. Mandava
A. Ted Watson
Department of Chemical Engineering
Texas A&M University
College Station, TX 77843

Carl M. Edwards
Engineering Imaging Laboratory
Texas Engineering Experiment Station
College Station, TX 77843

Introduction

Noninvasive imaging methods, such as X-ray CT scanning and magnetic resonance imaging (MRI), are providing exciting new opportunities for determining accurate rock characterizations and fluid-phase distributions corresponding to local regions within porous media. While much of the work reported for imaging methods have centered around the use of X-ray CT scanning (Potter and Groves, 1989; Vinegar, 1986), the versatility of MRI provides some unique opportunities for even more accurate and complete characterization of many properties associated with fluid-solid systems.

Most of the work to date has dealt with static or nonflowing situations. When the porous media contain a single fluid phase, the void volume of the media can be characterized by imaging (Edelstein et al., 1988). MRI can also be used to characterize the distribution of one or more fluid phases in multiphase situations (Hall and Rajanayagam, 1987; Chen et al., 1988; Baldwin and Yamanashi, 1986; Blackband et al., 1986). In previous studies, fluid distributions have typically been expressed by a quantity proportional to the intensity of the signal. While these experiments demonstrate the use of imaging, they provide at best only a semiquantitative measure of rock properties and fluid-phase distributions. Porosity and fluid saturations, which are desired for quantitative analysis of fluid transport and storage in porous media, have been reported only as averages for whole samples (Edelstein et al., 1988), rather than resolved spatially in one or more dimensions.

Several studies that deal with experiments involving transient multiphase flow in porous media have been reported (Baldwin and Yamanashi, 1986; Chen et al., 1988). Standard two-dimensional (slice) imaging procedures were typically used. In some cases, such as the absorption of water by nylon (Blackband and Mansfield, 1986), the flow process is sufficiently slow so that the time required for imaging is not a critical issue. In other cases, the flow has been disrupted to perform the imaging under static conditions (Chen et al., 1988; Baldwin and Yamanashi, 1986). This generally is not desired for quantitative work since some redistribution of fluid phases is to be expected.

In this work, we investigate the use of MRI for monitoring multiphase displacement experiments. In our experiments, one fluid phase is immiscibly displaced from a porous medium by a second fluid phase. Our objective is to accurately measure quantities that may be used to characterize the porous media and transport processes—specifically, the porosity and saturation profiles (i.e., the distributions along a single spatial dimension) in the direction of overall fluid flow. These quantities may in turn be used to estimate relative permeability and capillary pressure curves (Richmond and Watson, 1990), which are basic petrophysical properties used to describe the flow of multiple immiscible fluid phases in porous media. The profiles represent quantities which are averaged across the core transverse to the direction of fluid flow and are consistent with variables that appear in the usual one-dimensional macroscopic representation for flow in porous media. Such profiles can be obtained rapidly with the imaging method reported. The accuracy and resolution of the imaging method are developed in light of the challenge of imaging fluids that characteristically exhibit broad NMR linewidths, as do fluids in porous media.

Experimental Studies

The porous medium used was a solid cylindrical core, 0.0762 m in length and 0.0254 m in diameter, drilled from a block of limestone. The core was initially evacuated and then saturated with *n*-octadecene, the nonwetting phase. The core was inserted

into a rubber sleeve mounted in a plastic cell. A gas pressure of 1 MPa was maintained around the sleeve to ensure that there is no liquid flow from the core circumference. At the exit end of the core, a 0.0254 m spacer ring was placed between the core's surface and the end plate. The imaging of the displacement was conducted with a 2-Tesla GE NMR imager/spectrometer with a clear bore of 0.31 m and equipped with 0.2 Tesla/m shielded gradient coils. The core in its holder and an agarose reference sample taped onto the core holder were placed in the 0.11 m birdcage transmit/receiving coil in the horizontal bore of the NMR imager. Once fixed, the core and the reference sample were not moved throughout the entire experiment. The reference sample used was a gel of 16% agarose powder and 84% deionized water by weight (Mitchell et al., 1986).

The flow is through the core along its length in the same direction as the static field of the NMR magnet. To start with, the core was flooded with the nonwetting phase to ensure that the core was fully saturated with the oil before displacing it with the wetting phase. Deuterium oxide (D_2O), which does not emit a NMR signal at the proton resonance frequency, was used as the wetting phase to distinguish between the two phases. The D_2O used was of a minimum purity of 99.9 atom % D. Displacement of a saturating nonwetting phase with a wetting phase is termed primary imbibition. The flow rate was approximately 6×10^{-5} pore volumes per second during the initial part of the displacement. After the start of D_2O production from the exit end of the core, the flow rate was raised to about 2×10^{-3} pore volumes per second to speed up the displacement process. The displacement experiment was continued until no further changes in saturation were observed.

Imaging Procedures

The timing diagram of the principal imaging technique, shown in Figure 1, is a simplification of the spin-warp technique (Rothwell, 1985). In our case, the initial slice selective, narrow band radio frequency (RF) pulse is replaced by a nonselective broad band 90° RF pulse to excite the proton magnetization in the entire sample. The second RF pulse refocuses the spins in a spin echo. The gradient is applied in the sample's axial direction and is centered around the spin echo during signal acquisition. Care is taken to ensure that all the spins are in phase at the spin

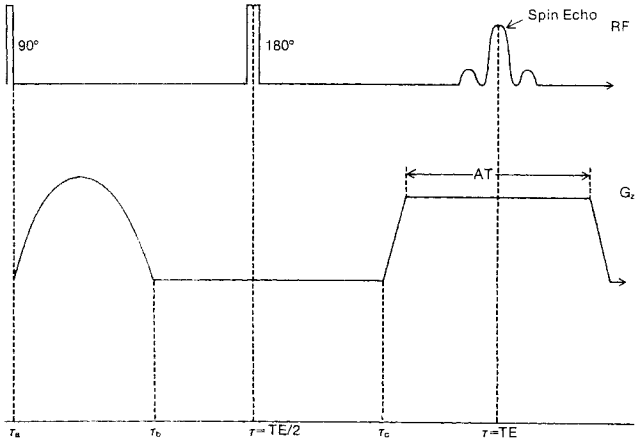

Figure 1. Timing diagram.

echo by requiring that

$$\int_{\tau_a}^{\tau_b} G(\tau)\, d\tau = \int_{\tau_c}^{TE} G(\tau)\, d\tau \tag{1}$$

where G is the magnitude of the gradient vector in the direction of the static magnetic field. The phase encoding gradients present in the spin-warp technique are eliminated.

In this experiment, the total time required to execute the pulse sequence and to acquire data for a single measurement of the one-dimensional spatial distribution of magnetization along the direction of the static magnetic field equals the echo time, typically of the order of milliseconds. If signals are coadded, the imaging time is approximately given by the product of the repetition time between two consecutive RF pulse sequences and the number of acquisitions less one. In our experiments, we coadded four signals and used a repetition time of 2.5 s so that the time used to acquire an image was approximately 7.5 s. This is considerably less than that required to obtain even a single two-dimensional image by the spin-warp method. The experimental time required for the two-dimensional image exceeds that of a profile by at least a factor of the number of phase encode steps required to encode the second dimension, typically 128 or 256. The profile images are better suited for observing the dynamics of the displacement experiment. This and other similar techniques have been used to measure gas-liquid density profiles (Shimokawa and Yamada, 1985), foam drainage profiles (Assink et al., 1988; German and McCarthy, 1989; McCarthy, 1990), and fluid adsorption in various materials (Blackband and Mansfield, 1986; Gummerson et al., 1979).

Porosity and Saturation Determination

We are interested in quantitative estimates of the porosity and fluid saturation distributions from the measured profile images. Fluids in porous media typically exhibit very short T_2 relaxation times and broad linewidths; these characteristics may limit the accuracy with which properties are estimated. The short transverse relaxation times and broad linewidths are due primarily to two factors. The heterogeneity of the fluid geometry and the difference between the static susceptibility of the rock matrix and fluid cause the lines to be broadened by approximately 3 $H_o \Delta\chi$ (Glasel and Lee, 1974; Drain, 1962). Increased surface relaxation rates caused by paramagnetic ions on the rock surface, and the presence of a fluid layer where molecular rotation is hindered, shorten T_2 and contribute to line broadening as well (Glasel and Lee, 1974). In this section, we examine the determination of porosity and saturation distributions from profile images. In the next section, we examine expected resolution and accuracy.

In the usual analysis of a profile image, the signal intensity in the frequency domain is given by

$$I_o(\omega) = k\mathbb{S}(z), \tag{2}$$

with

$$\mathbb{S}(z) = \int_{A_{xy}} \rho(x, y, z)\, dx\, dy, \tag{3}$$

and

$$\omega = \gamma G z. \tag{4}$$

The linear density $\mathbb{S}(z)$ is the number of hydrogen nuclei (protons) per unit length in the sample, and Eq. 4 provides a relation between the frequency and position in the sample. When $\mathbb{S}(z)$ is determined, the fluid-phase saturation can be calculated by

$$S_o(z) = \frac{\mathbb{S}(z)}{\mathbb{S}_i(z)}, \tag{5}$$

where $\mathbb{S}_i(z)$ corresponds to the linear density determined while the core is fully saturated prior to displacement. The porosity can be calculated by

$$\phi(z) = \frac{\mathbb{S}_i(z)}{nA_{xy}} \tag{6}$$

where n is the proton density of the observed phase.

To determine the linear density it is important to include a reference sample in the experimental volume. This enables the factor k in Eq. 2 to be determined. The factor k depends on many quantities, such as the receiver gain, the static magnetic field, and most importantly the quality factor, $\mathcal{Q}$, of the receiving coil (Abragam, 1961). $\mathcal{Q}$ is a measure of the energy losses in the receiving coil. While the receiver gain may change only slightly with time during a dynamic experiment, $\mathcal{Q}$ may change significantly. Dielectric losses and magnetic losses are the important factors in determining $\mathcal{Q}$ (Hoult and Lauterbur, 1979, and references therein). Changing saturations will produce changes in the dielectric losses; and if one of the phases is conductive (e.g., a saline solution), the magnetic losses will change as well. By using a reference sample during imaging, the factor k can be determined at all times during the experiment regardless of any changes that may have occurred.

$\mathbb{S}(z)$ can be determined from the following equation obtained using Eq. 2,

$$\mathbb{S}(z) = I_o(\omega) \int_{\Delta z_r} \mathbb{S}(z)\, dz \Big/ \int_{\Delta\omega_r} I_o(\omega)\, d\omega, \tag{7}$$

provided certain experimental conditions are met. Those conditions are that the echo time TE should be much less than the transverse relaxation time T_2 and that the repetition time TR, the delay time between consecutive RF pulse sequences, should be much greater than the longitudinal relaxation time T_1. The first condition may not be easily met in situations involving fluids with very short transverse relaxation times, as is typical with porous media. The second condition can become a factor of concern when the desired experimental imaging time requires a repetition time approaching T_1.

If the conditions on TE and TR are not met, the intensity of the signal will be a function of TE and TR. This can be represented by:

$$I(\omega,\ TE,\ TR) = I_o(\omega) g(T_1, T_2) \tag{8}$$

where T_1 and T_2 are the longitudinal and transverse relaxation times, respectively. The function $g(T_1, T_2)$ is in turn given by:

$$g(T_1, T_2) = e^{-TE/T_2} f(TR/T_1). \tag{9}$$

The function $f(TR/T_1)$ depends on the type of sequence used, but is approximately unity when $TR \geq 5T_1$. For a simple spin-echo pulse sequence, $f(TR/T_1) = 1 - \exp(-TR/T_1)$ (German and McCarthy, 1989). Using Eqs. 2 and 8, the linear density is given by:

$$\mathbb{S}(z) = \frac{I(\omega, TE, TR)}{\int_{\Delta\omega_r} I(\omega, TE, TR)\, d\omega} \frac{g_r(T_1, T_2)}{g_c(T_1, T_2)} \int_{\Delta z_r} \mathbb{S}(z)\, dz. \tag{10}$$

If TE and TR are not modified during the experiment and the relaxation times for the reference sample and the fluid in the core have been determined, the functions g_r and g_c can be calculated using Eq. 9. The linear density could then be determined, and the porosity and saturation profiles calculated. The knowledge of the relaxation times would not be required if only the saturations were desired, since the functions g_r and g_c will cancel as the ratio of Eq. 10 is formed with the corresponding equation for the fully saturated core prior to the displacement. It is possible that T_1 and T_2 of the core could be functions of saturation, but we have not addressed that problem here. For a fixed set of imaging parameters, we assume g_c to be constant. In our experiment, we use an agarose reference sample (Mitchell et al., 1986) that has been prepared to match the apparent T_1 and T_2 values for the fluid saturated core. By choosing a reference sample with relaxation parameters that match the experimental sample, errors that may be encountered when using Eq. 9 or in determining the relaxation parameters can be mitigated. The ratio $g_r(T_1, T_2)/\, g_c(T_1, T_2)$ was calculated using Eq. 9, with $f(TR/T_1)$ taken to be unity, to account for the mismatch in relaxation parameters.

Resolution and Accuracy

If the field gradients are sufficiently large and the linewidth sufficiently narrow so that $\gamma G \Delta z_p \gg 2\pi \Delta v_l$, the linear density at any location can be determined by the intensity at a corresponding frequency (see Eqs. 2–4). In this case, the maximum resolution

$$\Delta Z = \frac{2\pi \Delta f_p}{\gamma G}, \tag{11}$$

where Δf_p = (spectral width)/(number of pixels) is obtained. In porous media, the NMR linewidth tends to be very broad and thus tends to limit the resolution. In this section, we investigate the effect of signal broadening on the resolution.

In the rotating frame, the magnitude of magnetization in the presence of a linear gradient is given by (Rothwell, 1985)

$$M(r, t) = M(r, 0) \exp\{-i\gamma \vec{G} \cdot \vec{r}\, t - t/T_2^*\}. \tag{12}$$

T_2^* is the effective decay time of the transverse magnetization due to all line broadening mechanisms. The time domain signal

is given by the volume integral of the above function:

$$I(t) \propto \int_V M(r, 0) \exp\{-i\gamma Gzt - t/T_2^*\}\, dV, \qquad (13)$$

where we have substituted Gz for $\vec{G} \cdot \vec{r}$. Since $M(r, 0)$ is proportional to the spin density function,

$$I(t) = k \int_V \rho(\vec{r}) \exp\{-i\gamma Gzt - t/T_2^*\}\, dV. \qquad (14)$$

Taking the Fourier transformation to get the frequency domain signal intensity, we obtain

$$I(\omega) = k \int_{-\infty}^{\infty} e^{i\omega t} \int_V \rho(\vec{r}) \exp\{-i\gamma Gzt - t/T_2^*\}\, dV\, dt. \qquad (15)$$

Interchanging the integrals and carrying out the time integral, the following is obtained:

$$I(\omega) = k \int_{\Delta z_c} \mathbb{S}(z)[P(\omega - \gamma Gz) + iQ(\omega - \gamma Gz)]\, dz \qquad (16)$$

where

$$P(\mu) = \frac{T_2^*}{1 + [T_2^*\mu]^2} \qquad (17)$$

and

$$Q(\mu) = \frac{T_2^*\mu}{1 + [T_2^*\mu]^2}. \qquad (18)$$

The real part of the signal is given by

$$U(\omega) = Re[I(\omega)] = k \int_{\Delta z_c} \mathbb{S}(z) P(\omega - \gamma Gz)\, dz. \qquad (19)$$

Note that according to Eq. 19, the proton density corresponding to all locations in the sample contributes to the signal at frequency ω, whereas when transverse relaxation is neglected, proton density at only a single location contributes to the signal at ω (see Eq. 2). Estimation of the function $\mathbb{S}(z)$ through an equation of the form given by Eq. 19 for each discrete frequency represented in the experiment could, in principle, lead to more accurate estimates of the linear density than by using Eqs. 2 and 4.

Next, we develop a criterion that should be met if accurate estimates of the linear density are to be obtained from the simpler analysis provided by Eqs. 2 and 4. The maximum resolution given by Eq. 11 will be approached if T_2^* is sufficiently large so that

$$\int_{\Delta z_c} P(\omega - \gamma Gz)\, dz \approx \int_{\Delta z_p} P(\omega - \gamma Gz)\, dz. \qquad (20)$$

Then, the signal intensity is given by the linear density corresponding to a single pixel so that Eqs. 2 and 4 are suitable representations of the experiment. Equation 20 will thus be a valid approximation when the ratio

$$R = \int_{\Delta\mu_p} P(\mu)\, d\mu \Big/ \int_{\infty} P(\mu)\, d\mu, \qquad (21)$$

where $\Delta\mu_p = \gamma G\Delta z_p$, is sufficiently near to unity. Suppose that we require $R \geq \alpha$, where α is a specified positive constant that does not exceed unity. Using Eq. 21 to calculate $\Delta\mu$, and relating this to distance, we obtain:

$$\Delta Z = \frac{2 \tan\left(\frac{\pi\alpha}{2}\right)}{\gamma G T_2^*} \qquad (22)$$

for the Lorentzian lineshape. If, for example, we set $\alpha = 0.9$, so that 90% of the integral of the Lorentzian corresponding to a frequency can be identified with a single pixel, we obtain

$$\Delta Z = \frac{12.6}{T_2^*\gamma G}. \qquad (23)$$

The actual resolution would then be the maximum value of ΔZ from Eqs. 11 and 22. Equation 22 may be somewhat conservative, since the idealized Lorentzian generally predicts a slower decay with frequency than what may be actually observed. Also, it is not necessary to consider all frequencies in Eq. 21; only those within the spectral width of the experiment are required. If a Gaussian lineshape is used in place of the Lorentzian, the following is obtained when $\alpha = 0.9$:

$$\Delta Z = \frac{2.79}{T_2^*\gamma G}. \qquad (24)$$

Since the linewidth is inversely proportional to T_2^*, it becomes apparent that Eqs. 23 and 24 provide quantitative criteria for the previously stated condition for use of Eqs. 2–4 (namely that $\gamma G\Delta z_p \gg 2\pi v_l$).

The choice of which expression (Eq. 23 or 24) is most appropriate will depend on the actual experimental lineshape. In a porous media, the Gaussian linewidth may be more appropriate. Drain (1962) has shown that one of the mechanisms for broadening NMR resonance lines in powder samples is due to the difference between the static susceptibility of the powder and that of the surrounding media. Resonance lines in porous media will be broadened by the same mechanism. Moreover, the lineshape will tend to be Gaussian in character due to the random nature of the fluid distribution. Thus, Eq. 24 is likely to be appropriate for porous media samples.

In a displacement experiment, the measured quantities corresponding to any specific location represent some average observation over the period of time that it takes to perform the imaging sequence. Thus, the time to take an image may limit the accuracy with which the saturation profile is determined. Here, we develop a criterion for the time over which an image is acquired, T_{exp}, to ensure that the accuracy of saturation determination is not limited by the dynamic nature of the experiment.

We desire that the error in estimation of saturation during dynamic displacement not be greater than that for static

experiments. This is met if

$$\max |S_o(z, t + T_{exp}) - S_o(z, t)| \leq \epsilon_s \qquad (25)$$

where ϵ_s is the error in estimating saturation in a static experiment. The following can be obtained using a material balance:

$$S_o(z,t + T_{exp}) - S_o(z, t) = \frac{1}{\phi \Delta z_p}$$
$$\cdot \left[\int_t^{t+T_{exp}} v_o\left(z - \frac{\Delta z_p}{2}, t\right) dt - \int_t^{t+T_{exp}} v_o\left(z + \frac{\Delta z_p}{2}, t\right) dt \right]. \qquad (26)$$

The superficial velocity of the observed fluid phase does depend on the saturation. A conservative bound for the difference between the integrals on the righthand side of Eq. 26 is provided by setting one velocity, say that at $(z - \Delta z_p/2)$, to zero, and the other velocity to the total superficial velocity v. Then, we find that

$$\frac{v T_{exp}}{\phi \Delta z_p} \leq \epsilon_s. \qquad (27)$$

Equation 27 provides a conservative constraint on experimental parameters to ensure that the accuracy of saturation determination is not limited by the dynamic nature of the experiment.

Discussion of Results

Figure 2 is a plot of signal intensity profiles at successive stages of imbibition. The peak to the left of the figure corresponds to the reference sample, the central rectangular portion from units 61 to 190 corresponds to the oil in the core, and the peak at the right corresponds to the free oil in the spacer next to the exit end of the core. Since our birdcage coil has a good quality in RF homogeneity over the entire coil volume, the assumption of homogeneity of Q can be justified, and placement of the reference at the side of the core sample should not cause errors. The abscissa of Figures 2, 3 and 4 represents length in pixels, with each pixel being about 5.6×10^{-4} m long.

The porosity profile is shown in Figure 3. The porosity was calculated with Eqs. 6 and 10. The T_1 and T_2 values of the oil saturated core were determined to be 0.446 and 0.0065 s,

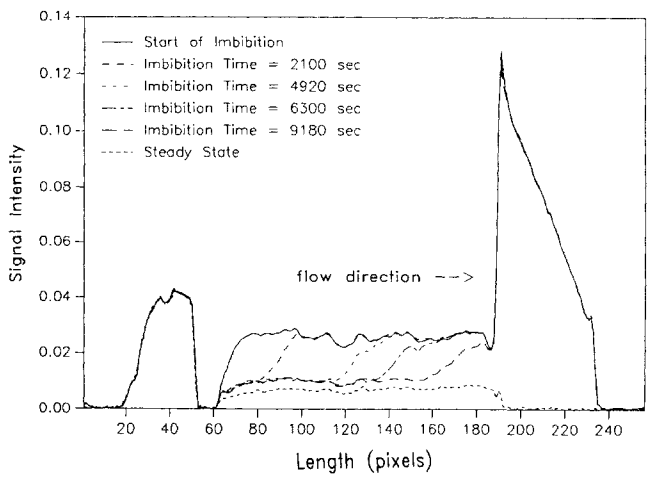

Figure 2. Profile images of imbibition experiment.

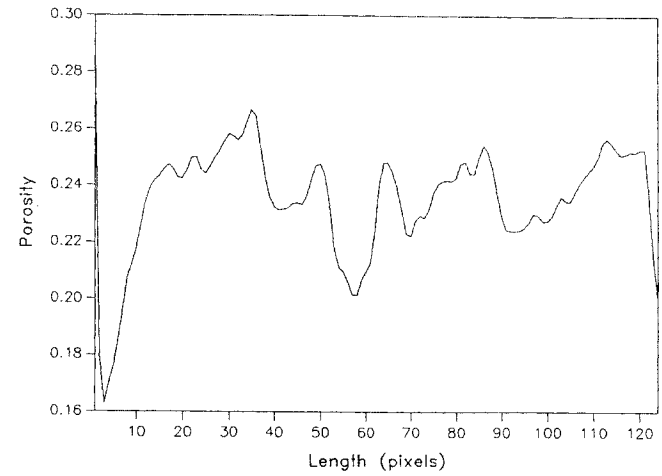

Figure 3. Porosity profile.

respectively. The corresponding T_1 and T_2 values of the reference sample were 0.398 and 0.0071 s, respectively. The ratio g_r/g_c, which is given by $\exp\{TE[(1/T_2^r) - (1/T_2^r)]\}$ when using unity for the function f in Eq. 9, was calculated to be 1.12. It should be noted that in experiments with fluids in porous media, TE (which is 0.009 s here) may be of the same order of magnitude as T_2. Proper selection of the reference sample becomes very important in such cases. For example, had one used a bulk fluid phase for the reference sample and not incorporated the correction factor, a 25% error in calculating the porosity would result. The average porosity obtained using the computed profile was 23.5%, which compares very well to a value of 23.1% obtained by gravimetric analysis.

The saturation profiles were calculated from Eqs. 5 and 10. As discussed previously, the factors g_r and g_c will cancel if parameters TE and TR are not modified, so the relaxation parameters are not necessary for determining the saturation profile. We used the average of 13 images to compute $\mathbb{S}_i(z)$ for use in Eq. 13. The saturation profiles are shown in Figure 4.

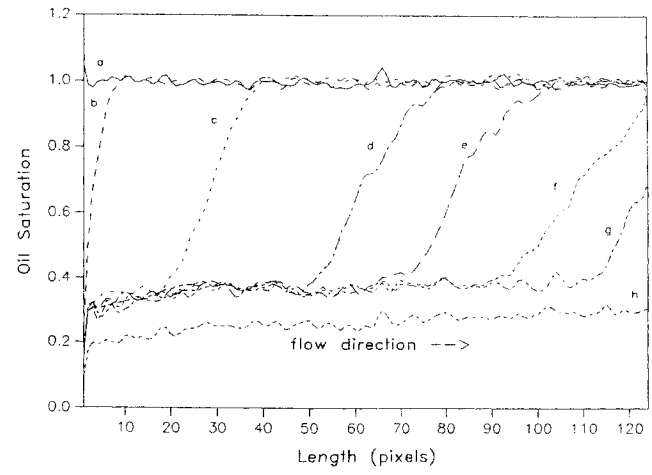

Figure 4. Nonwetting fluid saturation profiles.

Profiles correspond to different times during the experiment: a) before the start of imbibition; b) start of imbibition; c) 2,100 s; d) 4,920 s; e) 6,300 s; f) 9,180 s; g) 11,400 s; and h) steady state.

They appear to be consistent with what one might calculate for the one-dimensional displacement in uniform media.

The experimental data were analyzed to estimate the accuracy with which the saturation is determined. Data corresponding to two different saturation values were analyzed. The first case corresponds to the initial state (unity saturation) prior to the start of the displacement. Using 13 profiles, confidence intervals were obtained separately for each pixel. The confidence intervals were fairly uniform along the core. The median value of the confidence intervals was ± 0.015 saturation units. The accuracy corresponding to another saturation value was determined in a similar way by analyzing regions of 13 consecutive profiles during a period of time for which the saturation of the regions of the profiles were fairly uniform at a value of 0.36. The median value of confidence intervals, which was ± 0.013 saturation units, was very near to that determined for the other saturation value.

The maximum resolution for our experiment, calculated using Eq. 11, is 5.6×10^{-4} m. The ΔZ values calculated from the contribution of linewidths by Eqs. 23 and 24 are 3.1×10^{-4} and 7×10^{-5} m, respectively. Thus, our resolution for this experiment is 5.6×10^{-4} m. To investigate whether our accuracy is limited by the dynamic nature of the experiment, we calculate $\phi \Delta z_p \epsilon_s / v = 2.4$ s using the average porosity, a superficial velocity of 1.67×10^{-6} m/s, and a value of 0.03 saturation units for ϵ_s. Since this is about a third of our imaging time of 7.5 s, we cannot be assured that the accuracy of the determination of saturation in regions of fairly rapid change were not effected by the dynamic nature of the experiment. The requirements of Eq. 27 could be met if signals were not coadded. This would reduce the signal-to-noise ratio by about one half, with some deterioration in ϵ_s to be expected. The imaging time would be reduced substantially to about 0.01 s. It should be noted, however, that Eq. 27 represents a very conservative limit since the absolute value of the difference between the two velocities in Eq. 26 will always be much less than the superficial velocity v. Should our accuracy in estimating the saturation be limited by the dynamics of the experiment, it is likely to have occurred only in the region for which saturation is undergoing the greatest change, such as at the position for which the invading fluid first arrives at a given position. The maximum deterioration in the accuracy, as estimated by Eq. 27, would be ± 0.05 saturation units. Unfortunately, estimates of the relative permeabilities may be required for a better assessment of the accuracy when the conservative criterion given by Eq. 27 is not met.

Summary and Conclusions

We have addressed the quantitative determination of porosity and saturation profiles using NMR imaging of a dynamic displacement of immiscible fluids in a porous media. The use of a reference sample prepared to make its relaxation parameters match those for the fluid saturated core sample is demonstrated. The resolution for profile imaging was examined in light of the broad linewidths typically encountered when performing NMR spectroscopy in porous media. The effect of dynamic phenomena on the accuracy of estimation of the saturation profiles was investigated.

The resolution for our experiment was estimated to be 5.6×10^{-4} m. The accuracy, with which saturation is determined throughout most of the sample, was estimated to be ± 0.015 saturation units. The accuracy with which saturations are determined in regions which are undergoing the most rapid change in saturation may be less, but in any case would not exceed ± 0.05 saturation units.

Acknowledgment

The authors would like to thank Jim Mudra, Wen-Fu Hsu, and Dr. H. L. Chen for their help in the setup of the flow experiment.

Notation

A_{xy} = cross section of the experimental volume
f = correction factor in Eq. 9
Δf_p = spectral width of a pixel
g = correction factor in Eq. 8
g_c = correction factor corresponding to the core
g_r = correction factor corresponding to the reference sample
G = magnitude of the applied field gradient
$\vec{G}$ = gradient of the magnitude of the static magnetic field
H_o = magnitude of the static magnetic field
I = observed signal intensity
I_o = intrinsic signal intensity
k = constant of proportionality
M = magnitude of magnetization in the rotating frame
n = number density of protons in the observed fluid phase
P = real component of NMR signal
Q = imaginary component of NMR signal
Q = quality factor of receiving coil
$\vec{r}$ = location
R = ratio defined in Eq. 21
$\mathbb{S}$ = linear spin density
$\mathbb{S}_i$ = linear spin density corresponding to fully saturated core prior to displacement
S_o = saturation of observed fluid phase
t = time
TE = echo time
TR = delay time between consecutive RF pulse sequences
T_{exp} = time to acquire an image
T_1 = spin-lattice (longitudinal) relaxation time constant
T_1^c, T_1^r = spin-lattice relaxation time constant for the core and reference, respectively
T_2 = spin-spin (transverse) relaxation time constant
T_2^* = effective spin-spin relaxation time constant
T_2^c, T_2^r = spin-spin relaxation time constant for the core and reference, respectively
U = real part of the NMR signal intensity
v = superficial velocity
v_o = superficial velocity of the observed phase
V = volume
x, y, z = cartesian coordinates
Δz_c = length across core
Δz_p = length of a pixel
Δz_r = length across reference sample
ΔZ = spatial resolution

Greek letters

α = specified constant
γ = proton gyromagnetic ratio
ϵ_s = error in saturation
$\mu = \omega - \gamma G z$
$\Delta \mu_p = \gamma G \Delta z_p$
$\Delta \nu_l$ = full linewidth at half maximum
ρ = proton density (proton/m^3)
τ = time with respect to the imaging experiments
ϕ = porosity
$\Delta \chi$ = difference in static susceptibilities
ω = angular frequency
$\Delta \omega_r$ = angular frequency across reference sample

Literature Cited

Abragam, A., *The Principles of Nuclear Magnetism*, Oxford University Press, London (1961).

Assink, R. A., A. Caprihan, and E. Fukushima, "Density Profiles of a Draining Foam by Nuclear Magnetic Resonance Imaging," *AIChE J.*, **34**, 2077 (1988).
Baldwin, B. A., and W. S. Yamanashi, "Detecting Fluid Movement and Isolation in Reservoir Cores Using Medical NMR Imaging Techniques," SPE/DOE 14884, 39 (1986).
Blackband, S., and P. Mansfield, "Diffusion in Liquid–Solid Systems by NMR Imaging," *J. Phys. C: Solid State Phys.*, **19**, L49 (1986).
Blackband, S., P. Mansfield, J. R. Barnes, A. D. H. Clague, and S. A. Rice, "Discrimination of Crude Oil and Water in Sand and in Bore Cores with NMR Imaging," *SPE Formation Evaluation* (Feb. 1986).
Chen, J., M. M. Dias, S. Patz, and L. M. Schwartz, "Magnetic Resonance Imaging of Immiscible-Fluid Displacement in Porous Media," *Phys. Rev. Lett.*, **61**, 1489 (1988).
Drain, L. E., "The Broadening of Magnetic Resonance Lines due to Field Inhomogeneitics in Powdered Samples," *Proc. Phys. Soc.*, **80**, 1380 (1962).
Edelstein, W. A., H. J. Vinegar, P. N. Tutunjian, P. B. Roemer, and O. M. Mueller, "NMR Imaging for Core Analysis," SPE 18272, Houston (Oct. 2–5, 1988).
German, J. B., and M. J. McCarthy, "Stability of Aqueous Foams: Analysis Using Magnetic Resonance Imaging," *J. Agric. Food Chem.*, **37**, 1321 (1989).
Glasel, J. A., and K. H. Lee, "On the Interpretation of Water Nuclear Magnetic Resonance Relaxation Times in Heterogeneous Systems," *J. Amer. Chem. Soc.*, **96**, 970 (1974).
Gummerson, R. J., C. Hall, W. D. Hoff, R. Hawkes, G. N. Holland, and W. S. Moore, "Unsaturated Water Flow within Porous Materials Observed by NMR Imaging," *Nature*, **281**, 56 (1979).
Hall, L. D., and V. Rajanayagam, "Thin-Slice, Chemical Shift Imaging of Oil and Water in Sandstone Rock at 80 MHz," *J. Magn. Reson.*, **74**, 139 (1987).
Hoult, D. I., and P. C. Lauterbur, "The Sensitivity of the Zeugmatographic Experiment Involving Human Samples," *J. Magn. Reson.*, **34**, 425 (1979).
Mansfield, P., and P. G. Morris, *NMR Imaging in Biomedicine*, Academic Press, San Francisco (1982).
McCarthy, M. J., "Interpretation of the Magnetic Resonance Imaging Signal from a Foam," *AIChE J.*, **36**, 287 (1990).
Mitchell, M. D., H. L. Kundel, L. Axel, and P. M. Joseph, "Agarose as a Tissue Equivalent Phantom Material for NMR Imaging," *Magn. Reson. Imaging.*, **6**, 263 (1986).
Morris, P. G., *NMR Imaging in Medicine and Biology*, Oxford, Clarendon (1986).
Potter, G. F., and D. R. Groves, "Displacements, Saturations, and Porosity Profiles from Steady-State Permeability Measurements," SPE 19769, San Antonio (Oct. 8–11, 1989).
Richmond, P. C., and A. T. Watson, "Estimation of Multiphase Flow Functions from Displacement Experiments," *SPE Reservoir Eng.*, **5**, 121 (1990).
Rothwell, W. P., "Nuclear Magnetic Resonance Imaging," *Appl. Opt.*, **24**, 3958 (1985).
Shimokawa, S., and E. Yamada, Simultaneous and Direct Measurement of Gas–Liquid Density at High Temperature and High Pressure Using the Nuclear-Spin Projection Method," *Rev. Sci. Instrum.*, **56**, 1220 (1985).
Vinegar, H. J., "X-Ray CT and NMR Imaging of Rocks," *J. Pet. Tech.*, **38**, 257 (1986).

Manuscript received Apr. 3, 1990, and revision received Sept. 14, 1990.